Title:

Validation of backscatter measurements from the Advanced Scatterometer on Metop-A

Authors:

C Anderson, J Figa, H Bonekamp & JJW Wilson
EUMETSAT,
EUMETSAT-Allee 1,
D-64295 Darmstadt,
Germany.

J Verspeek & A Stoffelen
KNMI,
PO Box 201,
NL-3730 AE De Bilt,
Netherlands.

M Portabella
Unitat de Tecnologia Marina (UTM-CSIC),
Pg. Marítim de la Barceloneta 37-49,
08003 Barcelona,
Spain.

Corresponding Author:

Craig Anderson
email: craig.anderson@eumetsat.int
tel: +49 6151 807 7160

Abstract

The Advanced Scatterometer (ASCAT) on the Metop series of satellites is designed to provide data for the retrieval of ocean wind fields. Three transponders were used to give an absolute calibration and the worst case calibration error is estimated to be 0.15-0.25 dB.

In this paper we validate the calibrated data by comparing the backscatter from a range of natural distributed targets against models developed from ERS scatterometer data.

For Amazon rainforest we find that the isotropic backscatter decreases from -6.2 to -6.8 dB over the incidence angle range. The ERS value is around -6.5 dB. All ASCAT beams are within 0.1 dB of each other. Rainforest backscatter over a three year period is found to be very stable with annual changes of approximately 0.02 dB.

ASCAT ocean backscatter is compared against values from the CMOD-5 model using ECMWF wind fields. A difference of approximately 0.2 dB below 55 degrees incidence is found. Differences of over 1 dB above 55 degrees are likely due to inaccuracies in CMOD-5 which has not been fully validated at large incidence angles. All beams are within 0.1 dB of each other.

Backscatter from regions of stable Antarctic sea ice is found to be consistent with model backscatter except at large incidence angles where the model has not been validated. The noise in the ice backscatter indicates that K_p is around 4.5% which is consistent with the expected value.

These results agree well with the expected calibration accuracy and give confidence that the calibration has been successful and that ASCAT products are of high quality.

1. Introduction

The Advanced Scatterometer (ASCAT) is a European space-borne C-band radar instrument carried on the Metop-A satellite which was launched in October 2006 (Figa *et al.* 2002; Klaes *et al.* 2007). The instrument is designed to accurately measure the radar backscatter from the surface of the Earth. Over the ocean surface the backscatter characteristics are primarily influenced by the wind speed and direction and hence ocean wind vector information can be inferred from the radar measurements.

The main purpose of ASCAT is to provide estimates of the ocean wind vector to be exploited in weather fore- and nowcasting, ocean modelling and climate research applications. Operational wind services have been setup in the framework of the Eumetsat Polar System application ground segment. The ASCAT instrument is also exploited in other operational applications such as soil moisture retrieval (Bartalis *et al.* 2007) and sea ice mapping and drift measurements (Lavergne *et al*. 2010).

The accuracy of the retrieved geophysical information depends on the accuracy of the underlying radar backscatter measurements. These are expressed in terms of the Normalized Radar Cross-Section (NRCS), which is the ratio of the received backscattered energy to that of an isotropic surface scatterer as given by the two-way radar equation. NRCS measurements, denoted by σ_0, typically vary between -35 to -3 dB over the ocean for a wind speed range of 2 to 25 ms^{-1}.

The complete ASCAT commissioning process is described in the ASCAT Calibration and Validation Plan (Eumetsat 2004) and involves

- the setting of basic instrument and processing parameters,
- analysis of the gain patterns and calculation of calibration factors using transponders,
- validation of the backscatter from a variety of natural targets,
- validation of retrieved ocean winds against Numerical Weather Prediction (NWP) results and ocean buoy measurements.

The gain pattern analysis and results of the calibration are described by Wilson *et al*. (2010) and the validation of the retrieved ocean winds is given by Verspeek *et al*. (2010). Although the calibration and validation plan did not give any emphasis to cross-calibrations with other scatterometers (such as ERS1/2 and QuikSCAT), first comparisons with ERS-2 are given by Bartalis (2009).

The aim of this paper is to provide an overview of the calibration of the ASCAT and to assess the accuracy and stability of the NRCS measurements by means of geophysical validations.

In section 2 the ASCAT instrument and ground processing is briefly described. In Section 3 the external calibration with transponders is summarized and the key results on the accuracy of the σ_0 measurements, as elaborated by Wilson *et al*. (2010), are presented. Section 4 discusses the geophysical validation activities over rainforest, open ocean and sea ice. The latter are based on comparisons with established geophysical models. The performance of the ASCAT calibration against expectations is discussed in section 5.

2. ASCAT Instrument and Processing

The ASCAT instrument, described by Gelsthorpe (2000), is the follow-on scatterometer for the Active Microwave Instruments (AMI) on ERS-1 and 2. Like these, ASCAT operates at a frequency in C-band (5.3 Ghz) and the radar signal polarisation is vertical (VV). A major difference in design is that ASCAT comprises two sets of three fan beam antennas. One set points to the left of the sub satellite track and the other to the right so that measurements from two 550 km wide swaths located approximately 360 km left and right of the satellite ground track and covering an incidence angle range of 25-65° are obtained. This differs from the AMI which has only a single set of fan beam antennas covering a single swath with an incidence angle range of 19-55°.

In order to achieve a high range resolution, ASCAT transmits long pulses (of approximately 10 ms) with a linear frequency modulation at a carrier frequency of 5.225 GHz and with a peak power of about 120 W. The received echoes are low pass filtered, demodulated and fourier-transformed on board. The resulting spectra give the received power as a function of slant range.

Echo measurements are averaged along-track on board and passed, together with measurements of noise and internal calibration data, to the ground for further processing. The measurement mode processing consists of corrections to the raw power echoes (to remove range dependent receiver filter response, noise and instrument power gain variations), normalisation into NRCS values, and finally spatial averaging to obtain triplets of σ_0 estimates (corresponding to the three antenna beams) at the required locations. Two products containing spatially averaged backscatter values are produced:

- SZO in which the backscatter resolution is around 50 km and the backscatter values are calculated at 21 locations (termed nodes or wind vector cells) across the swath.

The spacing between nodes and between successive rows of nodes is approximately 25 km.

- SZR with a resolution of around 28 km, 41 nodes across the swath and a node spacing of approximately 12.5 km.

Details of the processing and products are described in the ASCAT Product Generation Function Specification (Eumetsat 2005) and the ASCAT Product Guide (Eumetsat 2009).

3. External Calibration

ASCAT is calibrated by means of three transponders which have been designed to provide stable and accurately known point target cross-sections. Each transponder tracks the Metop satellite during an overpass and when they receive the signal transmitted by the ASCAT they wait a fixed time interval before sending a signal of precisely known cross-section back to it. The transponders are located in Turkey and their position was carefully chosen to give optimum sampling of each antenna beam during the 29 day repeat cycle of Metop-A.

The calibration procedure has several steps. Firstly, the ASCAT data containing the transponder signal is processed to give the antenna gain value in the antenna coordinate system. This gives the antenna gain on a cut through the beam pattern at a particular elevation angle. An example of the raw ASCAT data containing a transponder signal is shown in figure 1 and an example of the antenna gain as a function of the normalised antenna azimuth angle is shown in figure 2. This process is repeated for a number of passes over the transponders at various elevation angles and a well sampled antenna gain pattern is obtained, as depicted in figure 3.

In the second step, a model of the antenna gain, antenna pointing error and gain pattern distortion is fitted to the set of data points. The residual between the data and the fitted model gives an indication of calibration accuracy.

In the third step of the process, the gain pattern models are used to obtain normalisation factors for converting the ASCAT measurements into absolutely calibrated backscatter. To do this we assume the Earth's backscatter to be unity and use the gain patterns to estimate the signal measured by ASCAT. Any differences between estimated and actual signal are taken to be a result of the Earths backscatter not being unity and dividing the actual signal by the estimated signal gives an estimate of the Earth's backscatter. Hence, the estimated signal is the required normalisation factor. These are calculated at various locations around the Metop-A orbit to take into account height and geometry variations.

Calibration campaigns, in which the transponders are operational and ASCAT is switched to calibration mode during every overpass, last approximately two months and are planned to take place every 18-24 months during the ASCAT lifetime.

The first campaign took place in November and December 2006, using the single transponder that was operational at that time. This gave a preliminary calibration and allowed products to be distributed as soon after launch as possible.

The second campaign, using all three transponders, took place during winter 2007-2008. The results from this campaign marked the end of the ASCAT commissioning phase and were used to reprocess older data as well as being applied to operational data. A description of this campaign and an initial investigation of the calibration quality are given in the ASCAT

Commissioning Quality Report (Eumetsat 2009). A more detailed report is given by Wilson *et al*. (2010) where an error analysis suggests a worst case around orbit calibration error of 0.15-0.25 dB.

4. Geophysical Validations

Geophysical validations form part of the ASCAT Calibration and Validation Plan (Eumetsat 2004). In these, the response from distributed natural targets is investigated to assess the quality of the backscatter. Geophysical validations can be performed over a variety of natural targets, e.g. rainforest, open ocean, sea ice and land ice. Validations over the global ocean have been used to derive bias correction coefficients which, when applied to the calibrated ASCAT data, bring it into alignment with the ERS based CMOD-5 ocean backscatter model (Verspeek *et al*. 2010). This was done in order to allow the retrieval of ASCAT winds soon after the Metop launch, using the only available backscatter model. These coefficients have been also used, until recently, to generate scatterometer soil moisture values from an ERS-based model (Bartalis *et al*. 2007). Geophysical validations are also routinely used to monitor the quality of the backscatter data produced by the operational ASCAT processor.

In this paper we report on validation results obtained from the 50 km resolution reprocessed backscatter data from the period 2007-2008 and the 50 km resolution operational data produced during 2009. This validation data set covers a period of three years.

4.1 Validation using rainforest backscatter

The backscatter from areas of rainforest has been extensively studied using the ERS-1 and ERS-2 scatterometers and has been found to be relatively stable. In particular the isotropic backscatter given by $\gamma_0 = \sigma_0/\cos\theta$ is found to be approximately constant with respect to time, viewing geometry and spatial location. An example of this as a function of incidence angle (taken from the ERS wind scatterometer cyclic report for cycle 42 in April to May 1999) is shown in figure 4. The region of Amazon rainforest used for monitoring ERS lies within longitudes -70 and -60.5° and latitudes -2.5 and 5° and the value of γ_0 given by ERS data is approximately -6.5 dB. Hence we can validate ASCAT data by taking ASCAT backscatter measurements from this region, calculating γ_0 and comparing it to the expected value.

Figure 5 shows the mean ASCAT γ_0 for the left hand antennas as function of incidence angle using all descending pass data during 2007 (which gives approximately 4300 samples at each value of incidence angle). The most obvious aspect of these plots is that ASCAT γ_0 is not a constant value close to -6.5 dB but instead decreases from approximately -6.2 to -6.8 dB over the incidence angle range. The γ_0 values in each of the three beams are similar with differences of at most 0.1 dB. This value does not completely represent the relative calibration between beams as it is also influenced by non-homogeneities in the rainforest and differences in viewing geometry. The mean γ_0 for the right hand antennas is shown in figure 6 and we find similar behaviour.

These results validate ASCAT to a certain extent as the -6.2 to -6.8 dB range for γ_0 encompasses the expected value of -6.5 dB. They also show that the relative calibration between beams is better than 0.1 dB. The behaviour of ASCAT γ_0 with incidence angle is unexpected as the γ_0 from ERS data is generally considered to be approximately constant across the incidence angle range. However, other authors have found dependencies on incidence angle. For example Zec *et al.* (1999) examine backscatter data from the Ku band NASA scatterometer (NSCAT) over the Amazon rainforest and model the incidence angle behaviour by fitting a third order polynomial. Their data shows that the Ku band backscatter over the rainforest changes from around -6 to -8 dB over an incidence angle range of 20 to 50°. These values of backscatter correspond to γ_0 values of -5.7 and -6.1 dB. This gives a change in NSCAT γ_0 of around -0.4 dB as the incidence angle increases from 20 to 50° and this very similar to behaviour we observe in ASCAT γ_0.

The stability of ASCAT is also of importance and can be examined using rainforest data. Figure 7 shows the mean γ_0 as a function of incidence angle for beam 1 (left mid beam) using data from the years 2007, 2008 and 2009. The difference between these is less than 0.02 dB which shows that both ASCAT and the annual averages of rainforest backscatter were very stable during this period.

Stability over shorter time scales is shown by the time series plot of rainforest γ_0 in figure 8. Each point in the figure shows the mean γ_0 at a particular incidence angle during a pass over the rainforest. The spread in γ_0 values is partly due to the incidence angle effect noted earlier in which larger incidence angles have lower γ_0 values.

However, there is another contribution to the spread caused by inhomogeneities in the rainforest. This is demonstrated by figure 9 which shows the geographical location of the near, mid and far range nodes in beam 1 ascending pass data during the years 2007 and 2008. These are not uniformly distributed across the region but cut through the rainforest at characteristic locations. Hence different incidence angles observe different parts of the rainforest.

Figure 10 shows the mean γ_0 along each of the near, mid and far range lines of nodes (red, blue and green symbols) as a function of the mean longitude. The different coloured symbols are displaced from each other in the vertical direction (showing variation of the γ_0 with incidence angle) but also show a characteristic variation with longitude which is caused by spatial variations in the rainforest.

Both of these factors need to be corrected in order to detect any small changes in the behaviour of ASCAT. The variation with incidence angle can be reduced by adding a node dependent bias correction so that the different coloured symbols in figure 10 are brought into alignment. The spatial variation can be reduced by adding a longitude dependent bias correction so that the γ_0 values become approximately constant. The bias corrected data is shown in figure 11 and shows very little variation with respect to incidence angle or longitude. A time series of the bias corrected data is shown in figure 12 and is less noisy than the original time series of figure 8. Seasonal variation in the rainforest of up to 0.2 dB can clearly be seen in this plot.

This method can be used to monitor the behaviour of the ASCAT calibration. Figure 13 shows a time series of the rainforest γ_0 in the left beam around September 2009 and we observe an unexpected step change of approximately 0.1 dB. This change is investigated in more detail in the next section.

The results presented in this section show that the calibrated ASCAT data over the rainforest has a similar value of γ_0 to ERS scatterometer data. However, the incidence angle behaviour is different, pointing to some differences in the ERS and ASCAT calibrations. The reasons for this need to be understood before merging of ERS and ASCAT data can take place to create a single data set with consistent characteristics. The results also show that γ_0 values from the individual ASCAT beams are within 0.1 dB of each other, which is consistent with the expected calibration accuracy. Yearly averages of rainforest backscatter are also found to be very stable, with changes less than 0.02 dB over the period 2007–2009.

4.2 Validation using ocean backscatter

Data from the ERS scatterometers has been used to develop a number of ocean backscatter models in which the backscatter is a function of incidence angle, wind speed and wind direction. The latest of these are CMOD5 (Hersbach 2003) and its equivalent neutral wind counterpart CMOD5.n (Hersbach 2008; Verhoef *et al*. 2008; Potabella & Stoffelen 2009). If the wind vector over the ocean is known, either from buoy measurements or from NWP models, then the output of the ocean backscatter model can be compared to the ASCAT data. Any bias between the two indicates either a difference between the ASCAT and ERS calibrations or to different biases in the input wind vectors (CMOD5 and operational European Centre for Medium Range Weather Forecasting (ECMWF) input are now found to produce backscatter values that are biased low for ERS data by about 0.5 dB (Verhoef *et al*. 2008) and this may be due to a bias in the ECMWF winds, which can be roughly removed by increasing them by about 0.5 ms^{-1}.) Variations on this approach have been developed and used by the Ocean and Sea Ice Satellite Application Facility (OSI-SAF), e.g. the NWP ocean calibration (NOC) and visual ocean calibration (VOC) methods (Verspeek *et al*. 2010).

Figure 14 shows the mean difference between the backscatter produced by CMOD-5 with ECMWF winds and ASCAT data over the open ocean during July 2009. The plots agree strongly with the results presented by Verspeek *et al*. (2010) and show two distinct types of behaviour.

Firstly, between 30-55° incidence the mean difference between ASCAT and the ERS based CMOD-5 is approximately constant at about 0.2 dB. This contrasts with the rainforest validation shown in the previous section which implies that the difference between ASCAT and ERS calibrations varies with the incidence angle.

Secondly, above 55° incidence the difference rises rapidly to about 1 dB. However, as CMOD5 was developed from ERS data covering the incidence angle range 19-55°, it seems likely this is a result of inaccuracies in CMOD-5 when extrapolated to large incidence angles rather than an indication of problems in the ASCAT calibration.

As CMOD-5 forms the basis for many wind vector retrieval algorithms this discrepancy at large incidence angles could potentially lead to large errors in the retrieved wind speed. However the approach taken by the OSI-SAF (Verspeek *et al*. 2010) circumvents this problem by applying bias correction factors to ASCAT data before wind retrieval.

The ocean validation can also be used to monitor the stability of the ASCAT. Figure 15 shows a time series over several years using the NOC calibration corrections (Verspeek & Stoffelen 2010). Note that the small step change in the calibration of the left mid beam during September 2009 has been provisionally corrected by subtracting 0.125 dB from September 2009 onwards. The ocean calibration residual (difference between measured backscatter and CMOD5.n simulated backscatter values obtained from the collocated NWP wind field) is in the order of 0.1 dB. The results from all beams are close together showing that interbeam variations are very small.

A seasonal variation is clearly seen in figure 15. This may be due to seasonal changes in the mean wind speed and mean stability at the buoys affecting the mesoscale wind variability. This would then cause some modulation in the spatial representation (wind component) errors as a function of season. As discussed in Stoffelen (1998) the random errors in wind components may cause apparent biases when comparing wind sensing systems with different random error characteristics.

These results show that the ASCAT instrument is very stable over time although there does appear to be a small downward trend. This may be due to changes in the operational ECMWF model over time (the forecasting system is updated twice a year). To verify such changes, the ASCAT winds are monitored against a set of buoy winds. The buoys cover the whole globe but are located mainly in the northern hemisphere and tropics.

Figure 16 shows evidence that over an extended set of Northern Hemisphere and tropical buoy winds collocated with ASCAT, the ECMWF model has been rather stable with a similar seasonal variation each year. There appears to be a small decrease in ASCAT wind speeds over this set of buoys, which is in line with figure 15, although further evidence is needed to support such subtle change.

It is also possible to use ocean backscatter to directly monitor the ASCAT calibration without the use of backscatter models, NWP or buoy winds. Figure 17 shows a section of width 0.4 dB through a three dimensional plot of the ASCAT backscatter triplets from the open ocean during August 2009. The data points tend to fall into two distinct regions, with higher and lower mid beam backscatter values. The *x* axis is then divided into bins of width 0.4 dB and the black circles show the location of the peak density of the data in the upper region of each bin. If the position of peak density is calculated for two separate months then a mean of the differences in the bins can be calculated. Figure 18 shows the mean difference for the months of August and November 2009 as a function of incidence angle and we find that there has been a change of approximately 0.1 dB between these two dates.

This approach can also be used to determine the date on which the change took place. If we calculate the position of the peak density using data from August 2009 then the number of ocean triplets in each orbit lying above and below this position should be approximately equal if the calibration remains constant. However, as shown in figure 19, a change occurs on September 11th 2009. The cause of this change has not yet been determined but it is not related to an upgrade to the ASCAT level 1b processor (which took place several days before this date) or to a satellite manoeuvre (which took place several days later).

The results presented in this section show that ASCAT data is within 0.2 dB of the value predicted by CMOD5.n with ECMWF equivalent neutral wind fields over incidence angle range 25-55°. This is consistent with the expected ASCAT calibration accuracies given by Wilson *et al*. (2010). Although the differences between the two become larger above 55° this may not be a reflection of the ASCAT calibration accuracy, but a result of possible inaccuracies of the CMOD5 model when extrapolated to this incidence angle range.

4.3 Validation using stable sea ice

Analysis of data from the ERS scatterometers has shown that backscatter from some regions of sea ice is approximately stable and can be accurately modelled. De Haan & Stoffelen (2001) find that the points given by plotting the fore, mid and aft backscatter from stable sea ice in a 3D measurement space form a line, with the position along the line being related to the "age" characteristic of the ice. This ice line model can easily be inverted to retrieve an estimate of the ice age from any backscatter triplet.

As we do not have prior information about the ice age we cannot use this model to give backscatter values that can be compared to ASCAT data. However, we can compare ASCAT data over stable sea ice to the model to see if they are consistent. Additionally, as sea ice is a relatively stable distributed target, we can use the backscatter from it to investigate the noise characteristics of ASCAT measurements.

In order to find regions of sea ice we bin ASCAT data in a polar grid and identify the grid cells where the RMS difference between the fore and aft beam backscatter is below a threshold of 0.5 dB. This strategy for locating sea ice is discussed and compared to other methods by Neyt *et al*. (2004). We then use the ice line model of de Haan & Stoffelen (2001) to retrieve the ice age for all the triplets in cells identified as sea ice. Cells in which the standard deviation of the ice age is below 0.5 are assumed to contain stable sea ice.

Sections through the three dimensional plot of the resulting stable sea ice triplets are shown in figures 20 to 22 for near range, mid range and far range of the left hand swath (i.e. for low, mid and high incidence angles).

At low and mid range incidence angles, the ASCAT data lies close to the model line. At larger incidence angles the data and model start to differ. However, as the ice line model was developed from ERS data covering the incidence angle range 19-55°, discrepancies between model and data above 55° are likely due to inaccuracies in the extrapolated model.

Fitting a straight line to the backscatter from stable sea ice and calculating the RMS distance between the data and line gives an estimate of noise in ASCAT measurements. Figure 23 shows the noise (converted to K_p) as a function of incidence angle. This is approximately 4.5% across the swath which is close to expected value of 3-4%.

The results presented in this section show that calibrated ASCAT data from regions of stable sea ice in the Antarctic is consistent with the ice line model at small and medium incidence angles which gives further confidence in the accuracy of the ASCAT calibration. At large incidence angles the ASCAT data and the model show discrepancies. However, this does not immediately point to any problem with the ASCAT data as the ice line model has not been validated over 55°.

5. Overall Summary and Conclusions

This paper describes the transponder based calibration approach for the ASCAT on Metop-A and presents the results from validations over natural targets using data from the period 2007-2009. The expected calibration accuracy of ASCAT has been estimated as 0.15-0.25 dB (Wilson *et al*. 2010) through an analysis of the residuals between transponder data and fitted gain patterns.

ASCAT backscatter over the Amazon rainforest has been validated by comparing the isotropic backscatter against the value of -6.5 dB given by ERS data. We find that the ASCAT values of γ_0 decreases from -6.2 to -6.8 dB over the incidence angle range of 25-65°. This difference in behaviour suggests there may be complications when constructing long term time series of ERS and ASCAT data. However the values from all ASCAT beams are within 0.1 dB of each other which is consistent with the expected calibration accuracy. Yearly averages of rainforest backscatter are found to be very stable with changes of about 0.02 dB over the period 2007–2009.

ASCAT data over the ocean has been validated by comparing it against the backscatter produced by CMOD-5.n with ECMWF equivalent neutral wind fields. This shows an approximately constant bias between the two of about 0.2 dB over incidence angle range 25-55°. This is inconsistent with the rainforest results. Although the data and model difference increases to around 1 dB at incidence angles larger than 55°, this is likely due to inaccuracies in CMOD-5.n, which has not been validated at large incidence angles. The relative inter-beam calibration is found to be about 0.1 dB.

Data from regions of stable sea ice in the Antarctic has been compared to the ice line model of de Haan and Stoffelen (2001) and the two are found to be consistent except at large incidence angles. However, as with CMOD-5, the ice line model was developed from ERS data and has not been validated over 55°. Hence, the discrepancy is likely due to inaccuracies in the model rather than the ASCAT calibration. An examination of the noise in the backscatter measurements of stable sea ice indicates K_p to be approximately 4.5% which is consistent with the expected value of 3-4%.

The results of these validation techniques are in agreement with the expected calibration accuracy of 0.15-0.25 dB, indicating that the ASCAT calibration has been successful and that ASCAT backscatter products are of high quality. However there are discrepancies between the various calibration methods: the ocean validation suggests the difference between ASCAT and ERS data is constant with respect to incidence angle while the rainforest validation suggests an incidence angle dependence. The rainforest validation also points to differences in the behaviour of ERS and ASCAT calibrations. These need to be investigated in more detail and understood in order find the optimum method for merging ERS and ASCAT data to create consistent data sets covering long time periods.

Finally, monitoring of ASCAT using rainforest and ocean data has shown that the instrument is extremely stable. An unexpected but small change in the calibration of the left mid beam occurred in September 2009. The reason for this change is not known and a more detailed analysis of new calibration data is currently underway and will correct any anomalies.

References

Bartalis Z., Wagner W., Naeimi V., Hasenauer S., Scipal K., Bonekamp H., Figa J., and Anderson C., 2007: Initial soil moisture retrievals from the METOP-A Advanced Scatterometer (ASCAT). *Geophys. Res. Letters*, **34**.

Bartalis Z., 2009: ERS-ASCAT backscatter and soil moisture inter-comparison - first results. ASCAT Soil Moisture Working Note No.6, IPF, Vienna University.

Eumetsat, 2004: ASCAT Calibration and Validation Plan. EUM.EPS.SYS.PLN.01.011.

Eumetsat, 2005: ASCAT Product Generation Function Specification. EUM.EPS.SYS.SPE.990009.

Eumetsat, 2009: ASCAT Product Guide. EUM.OPS-EPS.MAN.04.0028.

Eumetsat, 2009: ASCAT Commissioning Quality Report. EUM.MET.REP.08.0525.

Figa-Saldaña J., Wilson J.J.W., Attema E., Gelsthorpe R., Drinkwater M.R., and Stoffelen A., 2002: The advanced scatterometer (ASCAT) on the Meteorological Operational (MetOp) platform: a follow-on for European wind scatterometers. *Canadian J. Rem. Sens.*, **28**, 3, 404-412.

Gelsthorpe R.V., Schied E., and Wilson J.J.W., 2000: ASCAT-MetOp's Advanced Scatterometer. ESA Bulletin No. 102.

de Haan S., and Stoffelen A., 2001: Ice discrimination using ERS Scatterometer. Ocean and Sea Ice SAF report SAF/OSI/KNMI/TEC/TN/120.

Hersbach H., 2003: CMOD5 an improved geophysical model function for ERS C band scatterometry. ECMWF technical memorandum 395.

Hersbach H., 2008: CMOD5.N: A C-band geophysical model function for equivalent neutral wind. ECMWF technical memorandum 554.

Klaes D., Cohen M., Buhler Y., Schlüssel P., Munro R., Luntama J.P., von Engeln A., Clerigh E.O., Bonekamp H., Ackermann J., and Schmetz J., 2007: An introduction to the EUMETSAT polar system. *Bulletin of the American Meteorological Society*, **88**, 7, 1085-1096.

Lavergne T., Eastwood S., Teffah Z., Schyberg H., and Breivik L.A., 2010: Sea ice motion from low-resolution satellite sensors: An alternative method and its validation in the Arctic. *J. Geophys. Res.*, **115**, doi:10.1029/2009JC005958.

Neyt X., Pettiaux P., Manise N., and Acheroy M., 2004: Single pass sea-ice discrimination using ERS-2 scatterometer data. *Gayana*, **68**, 432-438.

Portabella M., and Stoffelen A., 2009: On scatterometer ocean stress. *J. Atm. Oceanic Technol.*, **26**, 368-382.

Stoffelen A., 1998: Toward the true near-surface wind speed: Error modeling and calibration using triple collocation. *J. Geophys. Res.*, **103**, C4, 7755-7766.

Verhoef A., Portabella M., Stoffelen A., and Hersbach H., 2008: CMOD5.n - the CMOD5 GMF for neutral winds. Ocean and Sea Ice SAF, technical note SAF/OSI/CDOP/KNMI/TEC/TN/165.

Verspeek J.A., and Stoffelen A., 2010: ASCAT NWP Ocean Calibration. KNMI/OSI-SAF report.

Verspeek J., Stoffelen A., Portabella M., Bonekamp H., Anderson C., and Figa-Saldana J., 2010: Validation and calibration of ASCAT using CMOD5.n. *IEEE Trans. Geosci. & Rem. Sens*., **48** 386-395.

Wilson J.J.W., Anderson C., Baker M.A., Bonekamp H., Figa-Saldaña J., Dyer R.G., Lerch J.A., Kayal G., Gelsthorpe R.V., Brown M.A., Schied E., Schutz-Munz S., Rostan F., Pritchard E.W., Wright NG., King D., & Önel Ü., 2010: Radiometric calibration of the advanced wind scatterometer radar ASCAT carried on board the METOP-A satellite. *IEEE Trans. Geosci. & Rem. Sens*., **48**, 8, 3236-3255.

Zec J., Long D.G., and Linwood-Jones W., 1999: NSCAT normalized radar backscatter coefficient biases using homogeneous land targets. *J. Geophys. Res*., **104**, 11557-11568.

Figures Captions

Figure 1: Image of a typical transponder signal recorded by ASCAT.

Figure 2. Antenna gain as a function of antenna azimuth angle derived from a single pass over a transponder in the left fore beam.

Figure 3. Depiction of antenna gain as a function of azimuth and elevation angles produced by data from multiple passes over the transponders.

Figure 4. An example of mean ERS γ_0 *as a function of incidence angle. This plot is taken from the ERS wind scatterometer cyclic report for cycle 42 (April to May 1999).*

Figure 5. Mean γ_0 *for the left hand beams as function of incidence angle using descending pass data from the year 2007.*

Figure 6. Mean γ_0 *for the right hand beams as function of incidence angle using descending pass data from the year 2007.*

Figure 7. Mean γ_0 *as a function of incidence angle for the left mid beam in the years 2007, 2008 and 2009.*

Figure 8. Time series plot of rainforest γ_0 *in the left mid beam for the years 2007, 2008 and 2009.*

Figure 9. The position of the near, mid and far range nodes (red, green and blue symbols, respectively) in the left mid beam in the rainforest test site during the years 2007 & 2008.

Figure 10. Mean γ_0 for the near, mid and far range nodes of the left mid beam (red, green and blue symbols) as a function of the mean longitude.

Figure 11. As figure 10 but with bias corrected data.

Figure 12. Bias corrected time series plot of rainforest γ_0 in the left mid beam for the years 2007-2009.

Figure 13. Bias corrected time series of γ_0 in the left mid beam for July to October 2009.

Figure 14. Mean difference between the backscatter produced by CMOD-5 (with ECMWF analysis winds) and ASCAT data from the right hand beams over the open ocean in July 2009.

Figure 15. Time series of ASCAT NWP ocean calibration residuals for each antenna. NOC corrections accumulated from Sep 2008 through Aug 2009 are applied (Verspeek & Stoffelen 2010). All level 1B backscatter changes are compensated by reverse corrections (Verspeek et al. 2010).

Figure 16. Time series of ASCAT and NWP buoy wind biases from a triple collocation data set. Level 2 changes have been compensated and all level 1B backscatter changes are compensated by reverse corrections (Verspeek et al. 2010).

Figure 17. Section along the x=y axis of a three dimensional plot where the x, y and z axes correspond to the fore, mid and aft backscatter from ocean σ_0 triplets. Small points show data from the left hand beams during August 2009 and large circles show the position of the maximum density of the data points in the upper region in bins along the x axis.

Figure 18. Mean difference between the positions of maximum density in data from August and November 2009.

Figure 19. Difference in the number of ocean triplets above and below the position of maximum density in each orbit during August and September 2009.

Figure 20. Backscatter from stable sea ice (circles) compared to the ice line model (dashed line) at the near side of the left hand swath.

Figure 21. Backscatter from stable sea ice (circles) compared to the ice line model (dashed line) at the centre of the left hand swath.

Figure 22. Backscatter from stable sea ice (circles) compared to the ice line model (dashed line) at the far side of the left hand swath.

Figure 23. K_p derived from standard deviation of stable sea ice backscatter around the best fitting straight line.

Figures

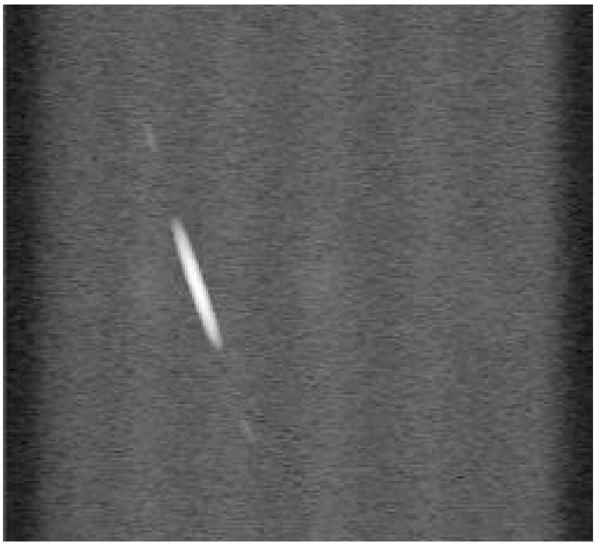

Figure 1: Image of a typical transponder signal recorded by ASCAT.

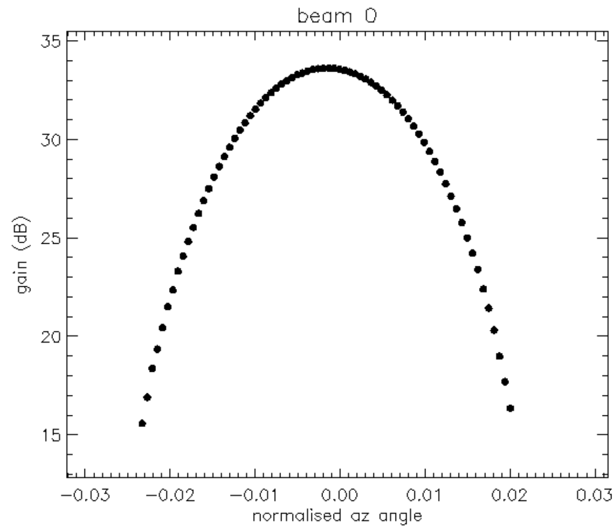

Figure 2. Antenna gain as a function of antenna azimuth angle derived from a single pass over a transponder in the left fore beam.

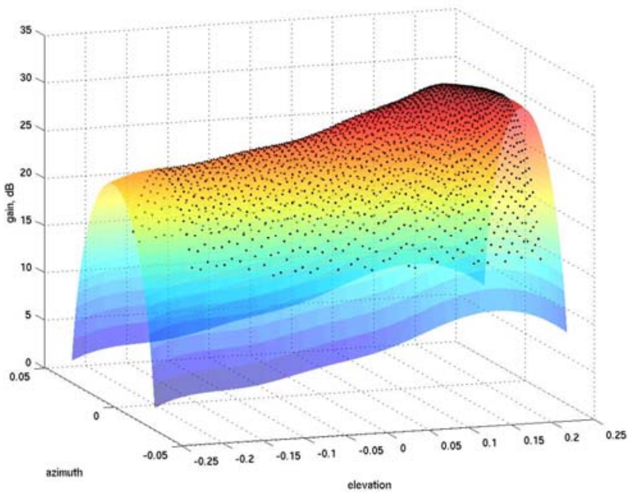

Figure 3. Depiction of antenna gain as a function of azimuth and elevation angles produced by data from multiple passes over the transponders.

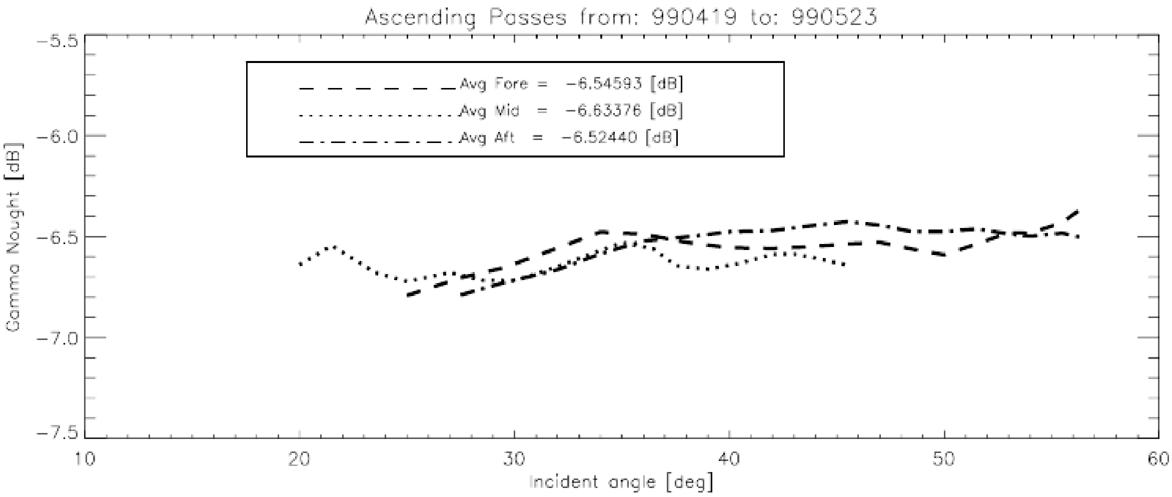

Figure 4. An example of mean ERS γ_0 as a function of incidence angle. This plot is taken from the ERS wind scatterometer cyclic report for cycle 42 (April to May 1999).

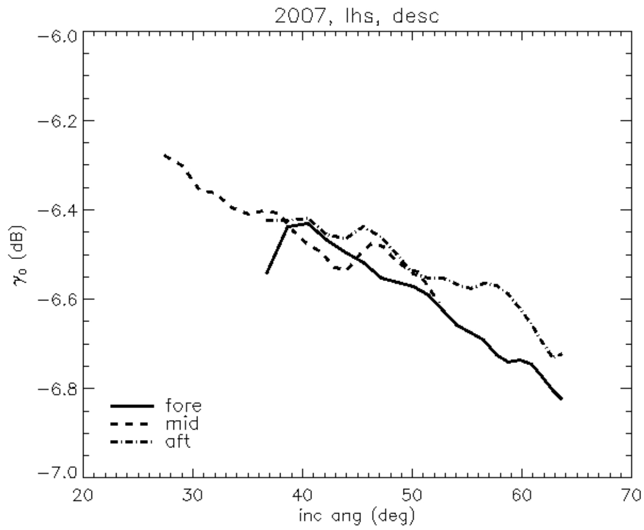

Figure 5. Mean γ_0 for the left hand beams as function of incidence angle using descending pass data from the year 2007.

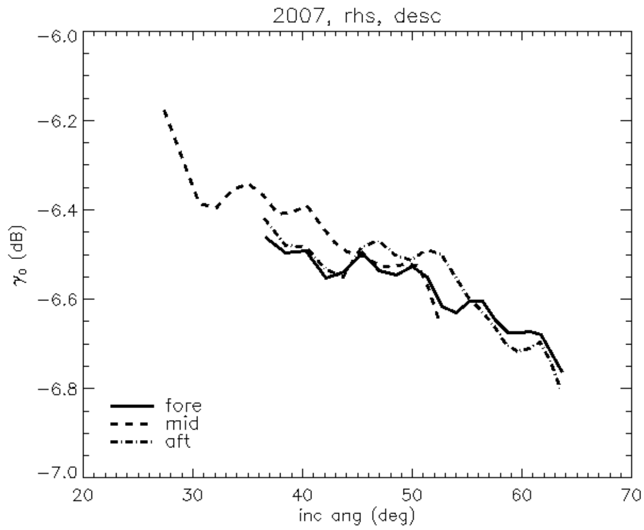

Figure 6. Mean γ_0 for the right hand beams as function of incidence angle using descending pass data from the year 2007.

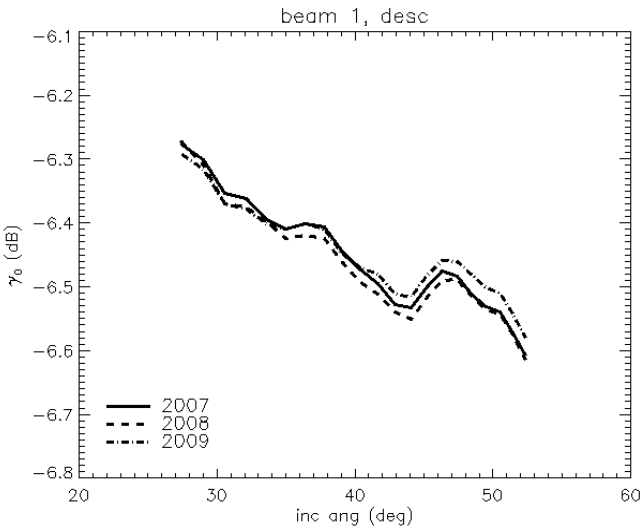

Figure 7. Mean γ_0 as a function of incidence angle for the left mid beam in the years 2007, 2008 and 2009.

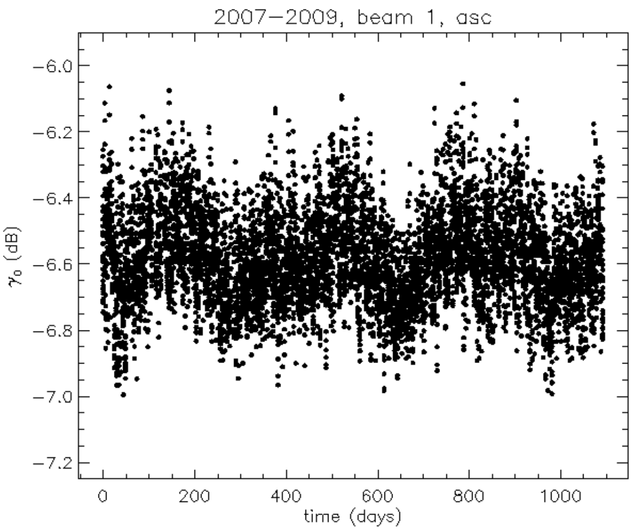

Figure 8. Time series plot of rainforest γ_0 in the left mid beam for the years 2007, 2008 and 2009.

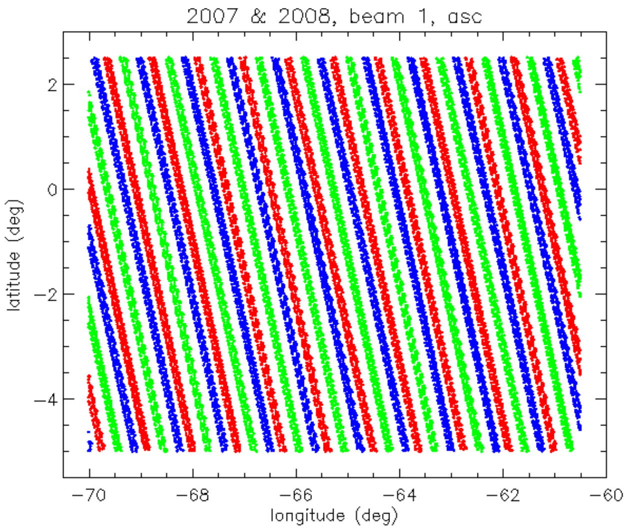

Figure 9. The position of the near, mid and far range nodes (red, green and blue symbols, respectively) in the left mid beam in the rainforest test site during the years 2007 & 2008.

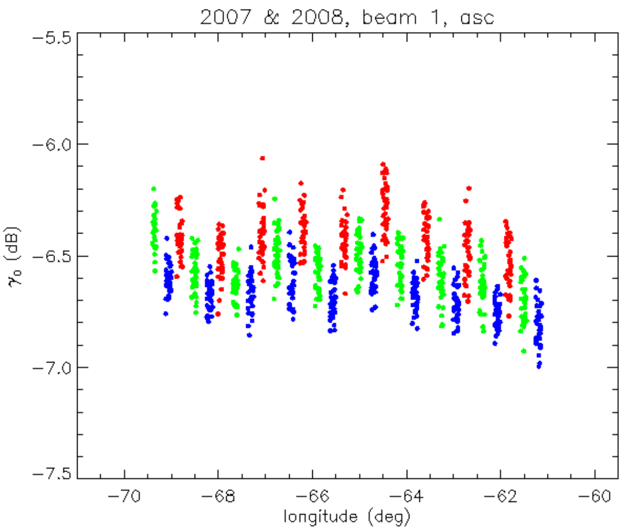

Figure 10. Mean γ_0 for the near, mid and far range nodes of the left mid beam (red, green and blue symbols) as a function of the mean longitude.

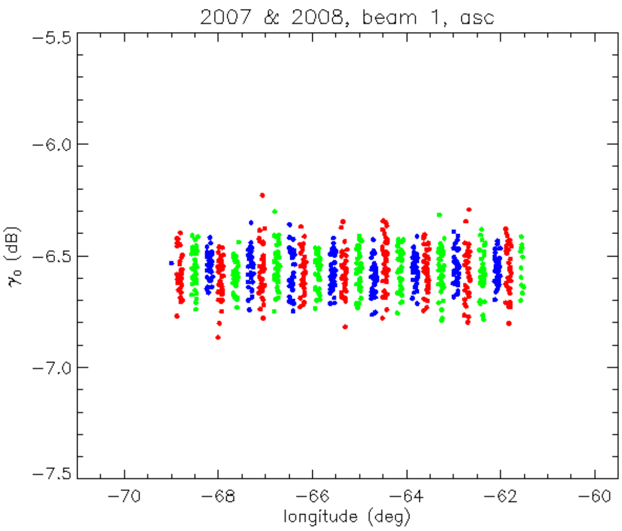

Figure 11. As figure 10 but with bias corrected data.

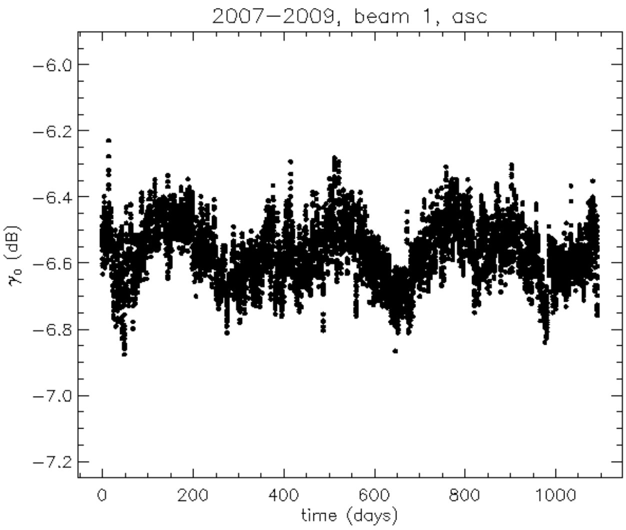

Figure 12. Bias corrected time series plot of rainforest γ_0 in the left mid beam for the years 2007-2009.

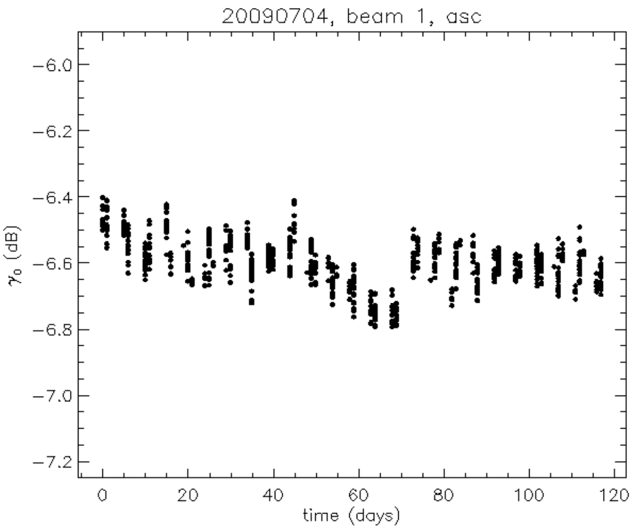

Figure 13. Bias corrected time series of γ_0 in the left mid beam for July to October 2009.

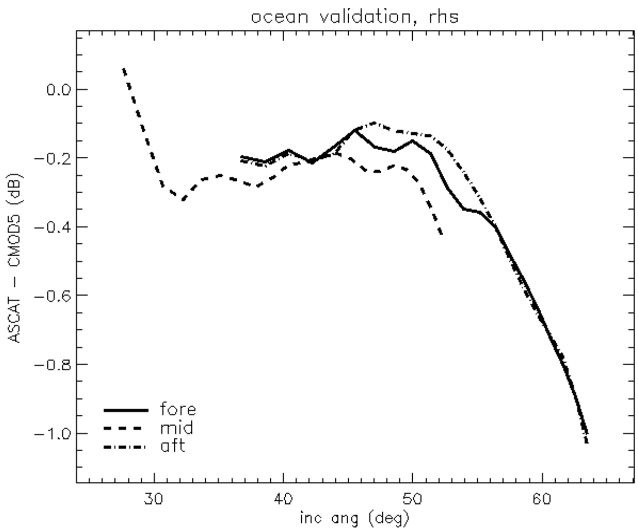

Figure 14. Mean difference between the backscatter produced by CMOD-5 (with ECMWF analysis winds) and ASCAT data from the right hand beams over the open ocean in July 2009.

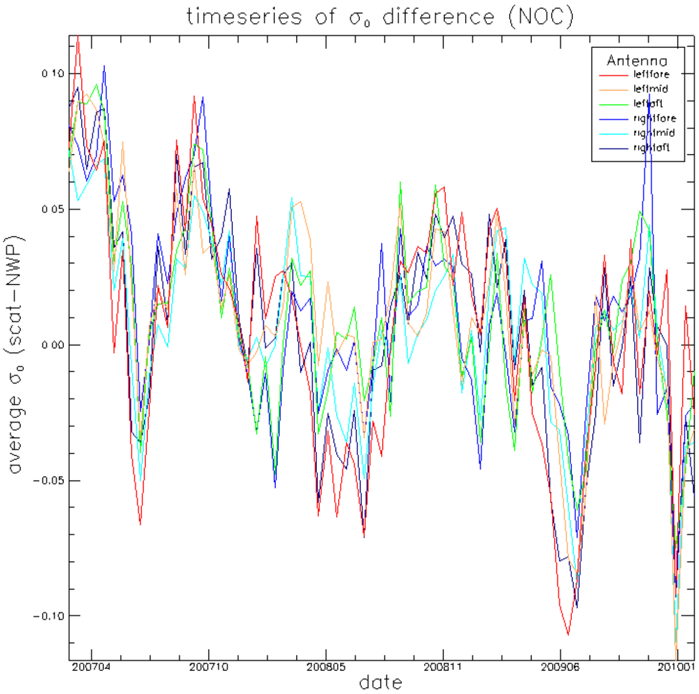

Figure 15. Time series of ASCAT NWP ocean calibration residuals for each antenna. NOC corrections accumulated from Sep 2008 through Aug 2009 are applied (Verspeek & Stoffelen 2010). All level 1B backscatter changes are compensated by reverse corrections (Verspeek et al. 2010).

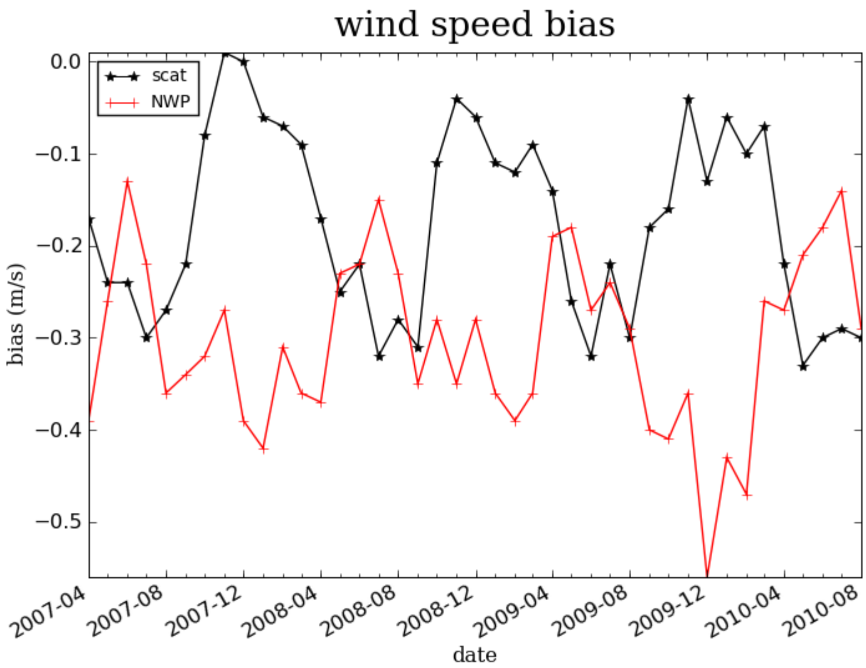

Figure 16. Time series of ASCAT and NWP buoy wind biases from a triple collocation data set. Level 2 changes have been compensated and all level 1B backscatter changes are compensated by reverse corrections (Verspeek et al. 2010).

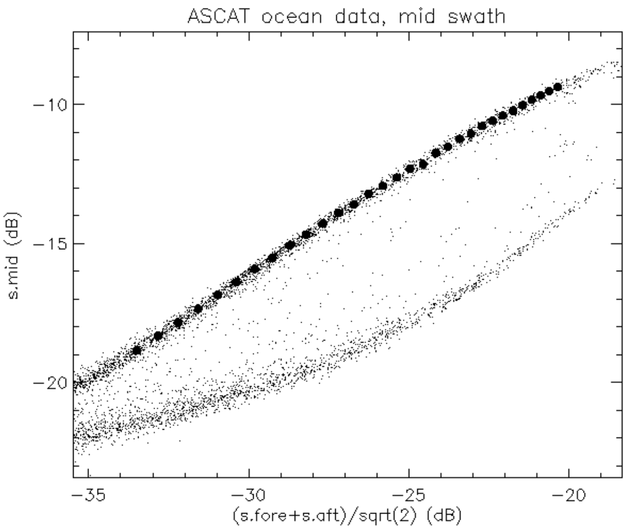

Figure 17. Section along the x=y axis of a three dimensional plot where the x, y and z axes correspond to the fore, mid and aft backscatter from ocean σ_0 triplets. Small points show data from the left hand beams during August 2009 and large circles show the position of the maximum density of the data points in the upper region in bins along the x axis.

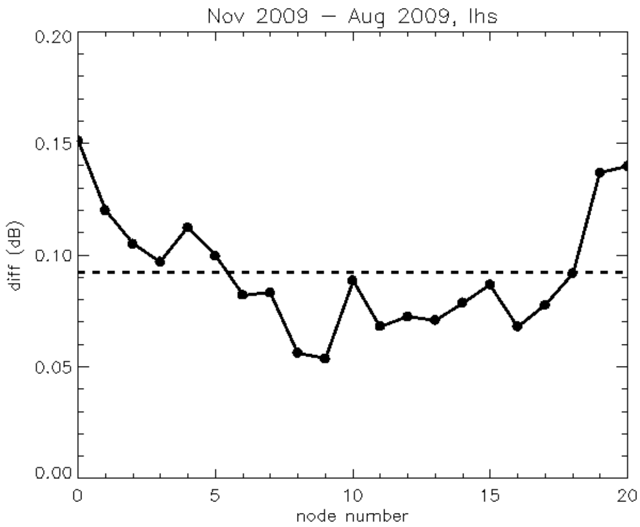

Figure 18. Mean difference between the positions of maximum density in data from August and November 2009.

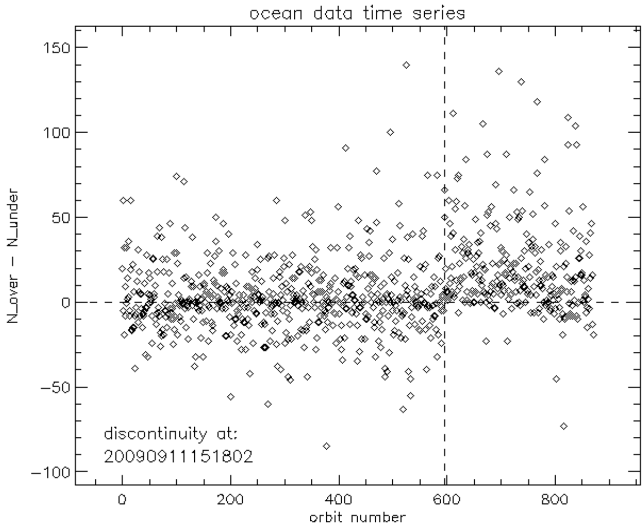

Figure 19. Difference in the number of ocean triplets above and below the position of maximum density in each orbit during August and September 2009.

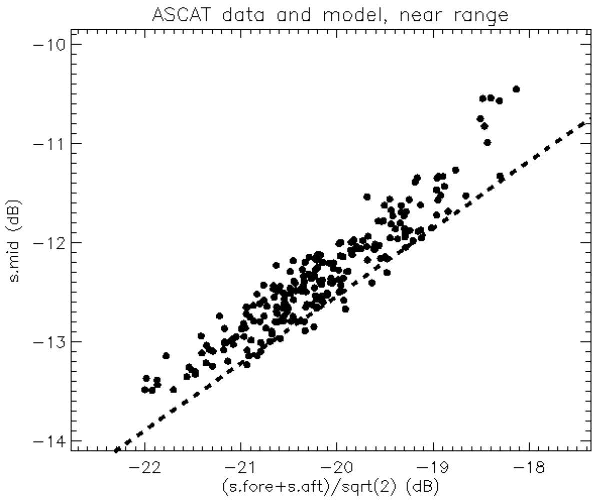

Figure 20. Backscatter from stable sea ice (circles) compared to the ice line model (dashed line) at the near side of the left hand swath.

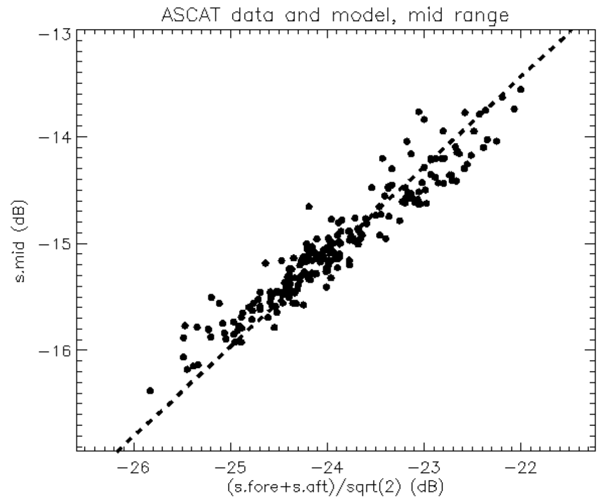

Figure 21. Backscatter from stable sea ice (circles) compared to the ice line model (dashed line) at the centre of the left hand swath.

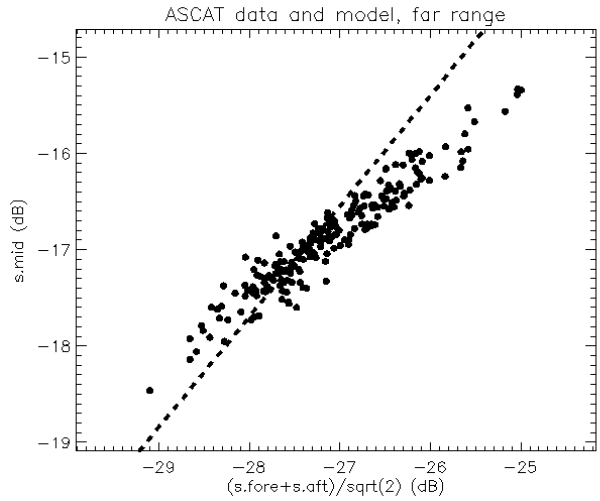

694

695 *Figure 22. Backscatter from stable sea ice (circles) compared to the ice line model (dashed*

696 *line) at the far side of the left hand swath.*

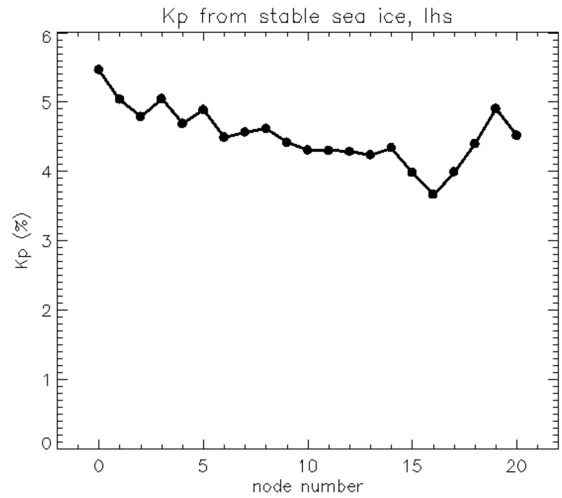

Figure 23. K_p derived from standard deviation of stable sea ice backscatter around the best fitting straight line.